Journal of Electroceramics, 15, 65–74, 2005

Influence of Defect Orientation on Electrical Insulating Properties of Plasma-Sprayed Alumina Coatings

S. BEAUVAIS,[1] V. GUIPONT,[1,*] M. JEANDIN,[1] D. JUVE,[2] D. TREHEUX,[2]
A. ROBISSON[3] & R. SAENGER[3]

[1] *Ecole Nationale Supérieure des Mines de Paris, Centre des Matériaux PM Fourt/UMR CNRS 7633- Centre de Compétence en Projection Plasma (C2P), BP 87, 91003 Evry Cedex, France*

[2] *Ecole Centrale de Lyon, UMR CNRS 5621, Ingénierie et Fonctionnalisation des Surfaces (IFoS), 69134 Ecully Cedex, France*

[3] *Schlumberger, Riboud Product Center, 1, rue Henri Becquerel, 92140 Clamart, France*

Submitted October 5, 2004; Revised March 15, 2005; Accepted March 22, 2005

Abstract. The influence of the microstructure (pores and cracks) on electric properties of plasma-sprayed alumina coatings was investigated using the so-called Scanning Electron Microscope Mirror Effect (SEMME) technique.

Coatings were sprayed with different alumina feedstock powders on various atmospheres using a CAPS ('Controlled Atmosphere Plasma Spraying'). Microstructures with various amount of porosity and cracks orientation distributions were analysed. Both outer surfaces and cross-sections of alumina coatings have been analysed by SEMME technique using two complementary modes (measurement of absorbed current and mirror methods). Originally developed to study the behaviour of injected electrons and related phenomena, such as trapping ability, detrapping process and relaxation phenomena in bulk insulating materials, the SEMME technique was successfully applied, in this study, to porous coatings. It is proved that cracks orientation modifies both motion and trapping of charges and therefore the dielectric properties of plasma-sprayed alumina coatings.

Keywords: plasma spraying, electrical properties, Al_2O_3, defects, SEMME method

1. Introduction

A ceramic coating obtained by thermal spraying can find applications as an electrical insulating layer for components of insulated high voltage electric devices or electronic sensors [1–4]. Among the existing insulating oxide ceramics for plasma spraying, alumina was chosen because of its high dielectric strength. Moreover, only high purity alumina powders (weight content >99%) were selected to achieve coatings with highest dielectric properties. Thermally-sprayed ceramic coatings exhibit a complex lamellar structure featuring a network of interconnected pores and cracks (interlamellar and intra-lamellar cracks typically). Consequently, the role of the porosity network is of great interest regarding the electrical properties of the coating (electrical permittivity, electrical breakdown strength). If a conductive medium like gaseous or liquid water is present within the pores, it could lower or even totally vanish the insulating properties [5]. Even in dry atmosphere, the influence of voids and cracks as diffusion barriers for conductive charges has been already discussed [6] and different effects have been observed [7, 8]. One example showed the low insulating properties determined for ceramic coating with very high thickness. In this case, it was claimed that influence of the coating thickness on the electrical resistivity was limited by the presence of numerous intra-lamellar cracks (perpendicular to the coating-substrate interface). These cracks were induced by the high thermal stresses always generated when very thick coatings are sprayed [7]. Other examples concerned 'dense' HVOF (High Velocity Oxy-Fuel) alumina coatings with different cracks densities or, compared to 'porous' APS (Air Plasma Spraying) alumina coatings [8, 9]. According

*To whom all correspondence should be addressed. E-mail: vincent.guipont@ensmp.fr

Table 1. Characteristics of alumina powders.

Powder	Size	Reference	Al_2O_3	NaO	Fe_2O_3	ZrO_2	SiO_2	CaO (*)
No. 1	$-70 + 20\ \mu$m	Snmi 22SN012	99.24	0.64	0.06	0.03	0.02	0.01
No. 2	$-25 + 10\ \mu$m	Metco 105 SFP	99.85	0.13	0.01	–	0.01	–
No. 3	$-12 + 2\ \mu$m	Amperit 740.090	99.94	0.04	0.01	–	0.01	–

*Chemical composition is given in weight%.

to these works, a porous coatings could have a higher relative permittivity than a dense coating but with numerous inter-lamellar cracks. Moreover, among HVOF coatings with similar porosity level, the lower electrical permittivity was measured on the sample with the highest amount of inter-lamellar cracks. These results evidenced the role of defects within thermally-sprayed coatings in dielectric properties. However, the influence of the microstructure on the insulating behaviour is not yet elucidated. The objective of this work was to investigate six microstructures with different porosity levels and cracks orientation distributions. These coatings have been sprayed using a CAPS facility ("Controlled Atmosphere Plasma Spraying") with different pressures and gases settings of the CAPS chamber as well as different alumina feedstock powder sizes. In order to investigate the behaviour of the electrical insulation and the influence of local defects on electric properties, the so-called Scanning Electron Microscope Mirror Effect (SEMME) technique has been used.

2. Experimental Procedure

2.1. Spraying Conditions and Materials

APS (Air Plasma Spraying) and HPPS (High-Pressure Plasma Spraying) alumina coatings were sprayed on grit blasted stainless steel plates (AISI 316L, 25 × 30 × 2 mm^3, Ra = 4 μm) using air (atmospheric pressure) and argon (250 kPa) with a F4-VB torch (nozzle internal diameter: 6 mm). Specimens were carried out using a multi-process CAPS facility (Sulzer Metco, Wohlen, Switzerland). In earlier works, it has been shown that HPPS could be successfully applied to a large range of ceramics up to 250 kPa of argon [10, 11]. With a better plasma-to-particles heat transfer under high pressure it might result in reducing coating porosity and/or in allowing better control and selection of coating microstructure. Three different alumina powders with large, medium and small particle size ranges were sprayed with the APS mode using the same plasma parameters. HPPS alumina coatings were achieved using the powder with medium particle size range. The characteristics of alumina powders are listed in Table 1. In the HPPS mode, three different plasma gas mixtures were used in order to promote low, medium and high electric effective plasma gun power (effective power is a significant plasma parameter because it involves pressure dependent heat losses through water-cooled gun nozzle). APS and HPPS plasma parameters are summarized in Table 2. In previous works [10], it was shown that the presence of α-Al_2O_3 in the CAPS coating was only due to the incorporation of unmelted α-Al_2O_3 particules. This result was ascertained by X-ray diffraction analysis. The γ-Al_2O_3 phase was the major phase in the APS and HPPS coatings.

Table 2. Plasma parameters for alumina coatings specimens and corresponding microstructure reference.

Spraying conditions	*#1*	*#2*	*#3*	*#4*	*#5*	*#6*
CAPS Mode	APS 100 kPa air			HPPS 250 kPa argon		
Power (kW)	14.5			12.5	19	22
Feedstock powder	1	2	3	2		
Feedrate (g.min^{-1})	20			20		
Spray distance (mm)	130			130	100	130
Injector diameter (mm)	1.8			1.1		
Coating thickness (mm)	0.2	0.6	0.2	0.1	0.3	0.3
Microstructure reference	*f*	*c*	*d*	*e*	*a*	*b*

2.2. Quantitative Image Analysis

Each coating's microstructure was quantified using image analysis of sets of SEM microstructures (LEO1450VP). To meet criteria for statistics, 25 SEM digitalized images (512 × 512 $pixel^2$) were recorded for each different coating. The back scattering electron mode was used to enhance the image contrast of voids

and defects present in the coatings. Cross-sectionned specimens were metalized (Au-Pd film) prior to SEM acquisition. Quantitative image analysis (QIA) consisted in multi-stage processing using "MATLAB®" software. One example of processing steps and corresponding series of working images for the pores and cracks contents investigation is given in Fig. 1. In this example, the image I is the starting original SEM image. By operating a threshold and subsequent background noise filtering the "whole porosity" (pores and cracks) image II is obtained. The binary "pore" image *V* used to calculate the globular pores content (in%) resulted in the intersection between the "whole porosity" image II and the binary image IV obtained after thresholding of the fuzzy image III (the fuzzy mode allowed to apply a Gaussian filter to image I which deleted small-sized objects such as cracks). The "cracks" image VI resulted in subtracting the "pores" image V from the "whole porosity" image II led to the cracks content (in%). The total porosity content (in%) was then quantified by adding the globular pores content to the cracks content.

Further "cracks" images were processed by a skeletizing procedure (limiting defects thickness to only 1-pixel) and deleting triple points and their first neighbouring points (not given in Fig. 1). From the thus-skeletized "cracks" image, both inter-lamellar cracks (main line orientation $<45^\circ$) and intra-lamellar cracks (main line orientation $>45^\circ$) could be defined and discriminated easily using an automatic orientation criterion. Oriented crack density could be then measured for both types of cracks through the counting of the number of cracks which were intersected by 100 μm-long segments. This resulted in average values expressed as numbers of cracks per length unit.

2.3. *SEMME Technique*

The scanning Electron Microscope Mirror Effect (SEMME) technique was originally developed to study the ability of a bulk insulating material to store electric charges without contact of electrodes. This technique has never been applied to porous thermally-sprayed ceramic coatings.

Principle: Although the SEMME method has been fully explained previously, the principle is briefly recalled [12–16]. The sample is irradiated by electrons at high voltage in a SEM (LEO 440) equipped with a beam blanking device. Primary beam intensity and irradiation time (t_{inj}) were adjusted in order to inject a well-known quantity of charges (Q_{inj}). The charges stored in the insulating material induce an image charge in the grounded metallic sample holder. On the other hand, electric charges trapped and locally stabilised near by the injection zone produce a strong electric field in the vacuum chamber of the SEM. These two features allow a characterisation of the trapping properties according to the two complementary methods respectively: the absorbed current measurement and the mirror method.

The absorbed current I_{ab}, produced between the sample holder and the ground during t_{inj} is recorded and measured using a picoammeter (Keithley 428). The absorbed current I_{ab} is strictly proportional to the total amount of charges stored within the insulator.

Typical $I_{ab}(t)$ curves obtained with the absorbed current method are represented in Fig. 2. Main characteristics of charges trapping and relaxation can be quantified:

- Q_{ab}, maximum quantity of trapped charges stored $I_{ab}(t)dt$ (pC) within the whole sample, is given by $Q_{ab} = \int_{t_0}^{t_{inj}} I_{ab}(t)dt$ (pC);
- t_r is the time before the first relaxation ($t_r < t_{inj}$), marked by a drop in I_{ab};
- Q_r is the quantity of charges stored before relaxation, $Q_r = \int_{t_0}^{t_r} I_{ab}(t)dt$ (pC).

According to the shape of $I_{ab}(t)$ curves, further information on the electric charges behaviour can also be obtained. The strong enough electric field deflects the incident electrons as a convex mirror does with light. In the SEMME technique, it is the field of charges trapped and stabilized at the beam impact point. Than subsequent observation of the irradiated zone is done using a low energy electrons beam (scanning potential V in the range 100 to 1000 V). A distorted view of the SEM chamber is displayed on the screen. By measuring the apparent diameter of the gun exit as a function of the scanning potential, the so-called mirror plot $1/d = f(V)$ is obtained and the quantity Q_t of trapped and stabilised charges can be deduced using the electrostatic law $1/d = (4L/d')(V/A.Qt)$ with L the working distance of the SEM (10 mm), d' the diameter of the exit gun (5.3 mm), d apparent diameter of the gun exit measured on the screen, V the scanning potential and A is parameter dependent on SEM chamber characteristics, thickness and permittivity of the insulating coating [12].

It is important that both absorbed current and mirror methods allow two different measurements of the

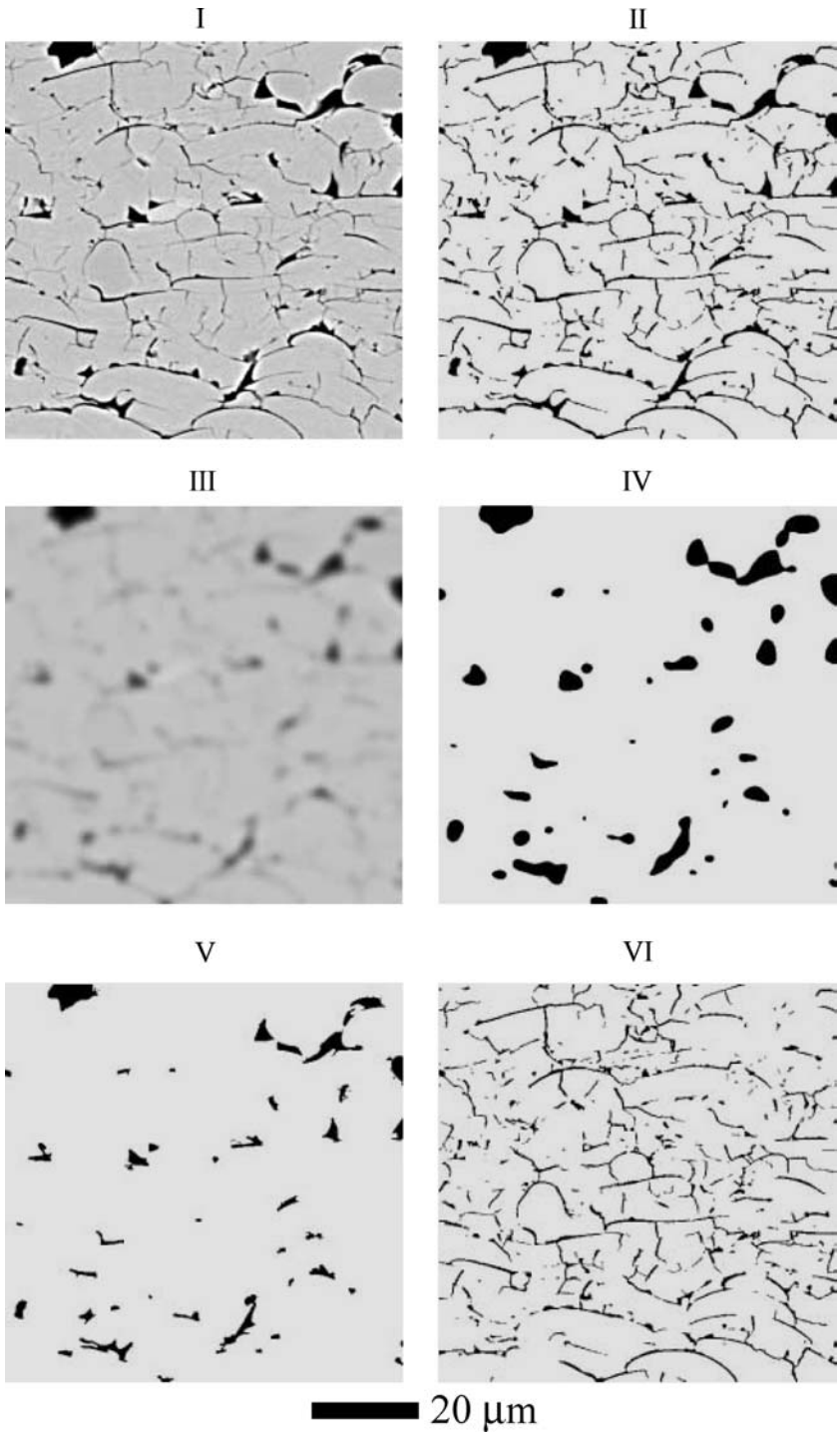

Fig. 1. Processed images for porosity and cracks assessment by QIA: I/original SEM image; II/pores and cracks binary image; III/fuzzy image; IV/ binary fuzzy image; V/"pores" image (intersection of II and IV); VI/"cracks" image (subtraction of V from II).

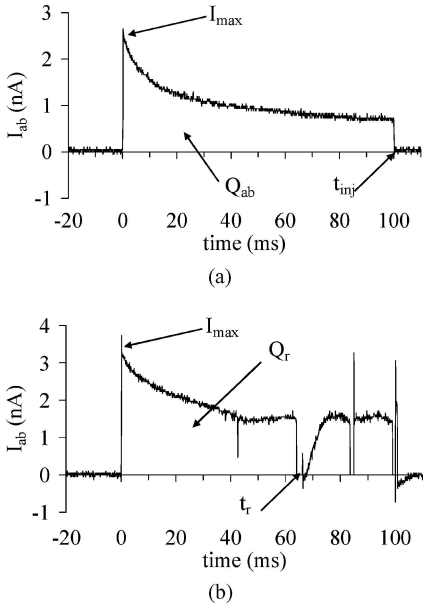

Fig. 2. Different parameters deduced from the absorbed current method: (a) curve without relaxation, (b) curve presenting charge relaxations.

quantity of charges, the main difference between the two parameters is that:

- in the first case, Q_{ab} represents the charges stored (trapped and stabilised or diffused) in the whole insulating material.
- in the second case, Q_t is a local quantity of the charges trapped and stabilised just beneath the beam impact point.

Experimental Procedure: Prior to experiments samples were ultrasonically cleaned in ethanol. Before testing, each sample was put in the SEM chamber and conditioned in vacuum during 3 hours at about 100°C to reduce the surface contamination.

Injections were performed using the following conditions: primary beam energy $E_0 = 30$ keV, primary beam current $I_0 = 500$ pA; t_{inj}: 100 ms. Injections ($Q_{inj} = 500$ pC) were done with an unfocused beam (30 μm in diameter) to ensure reliable characterisations of the heterogeneous microstructure of the coatings (including pore, cracks, bulk alumina, interfaces and grain-boundaries). Ten injections were performed on the surface of six different as-sprayed coatings. Further investigations (five injections) were made on polished cross-sections of two selected coatings.

3. Results and Discussion

3.1. Selected Microstructures

Six different alumina coatings were sprayed using two different CAPS modes: APS #1 to #3 and HPPS #4 to #6 (numbers refering to the spraying conditions that are given in Table 2). The respective influence on insulating properties of the main γ-Al_2O_3 phase and the residual α-Al_2O_3 phase was not considered in this work. It was assumed that the coating porosity (filled with air) was the predominant microstruture feature that could influence the dielectric behaviour.

The typical microstructures obtained according to the plasma conditions are shown on Fig. 3 (microstrutures a to f; letters refering to the parameters that are summarized in Table 2). The sets of SEM digital images allowed to measure the total porosity content (pores and cracks in%) and to achieve the quantitative study of the microstructure defects according to the QIA procedure described previously. The results, obtained with increasing porosity content for microstructures (a) to (f), are summarized in Fig. 4. QIA results for porosity were in good agreement with those measured by the immersion method [11]. In the APS mode, the coarser particle size led to the coating with the higher pores content. It could be explained by the rather large diameter of the spreaded particles ('splats') that might result in larger voids than smaller particles. Moreover, larger particles might be more difficult to heat and accelerate homogeneously. Therefore, highly porous material was obtained with the coarse powder. If the feedstock particle size was decreased, it was obvious the porosity level was drastically improved. But for the fine and medium sizes powders that has been sprayed in the APS mode, the resulting global porosity level was near similar.

If APS and HPPS coatings are compared together, it allowed to propose a variety of alumina coatings with different features regarding coatings defects (nature, content, orientation). The dense coatings were obtained using the powder No. 2 ($-25 + 10$ μm) in the HPPS mode with the two effective powers 19 kW (microstructure a) and 22 kW (microstructure b). A highly porous coating was also obtained with this mode but at a lower effective power (microstructure e). A rather similar highly porous coating was produced in the APS mode (microstructure f) using the powder No. 1 ($-70 + 20$ μm). The most dense coating using the APS mode was obtained with the

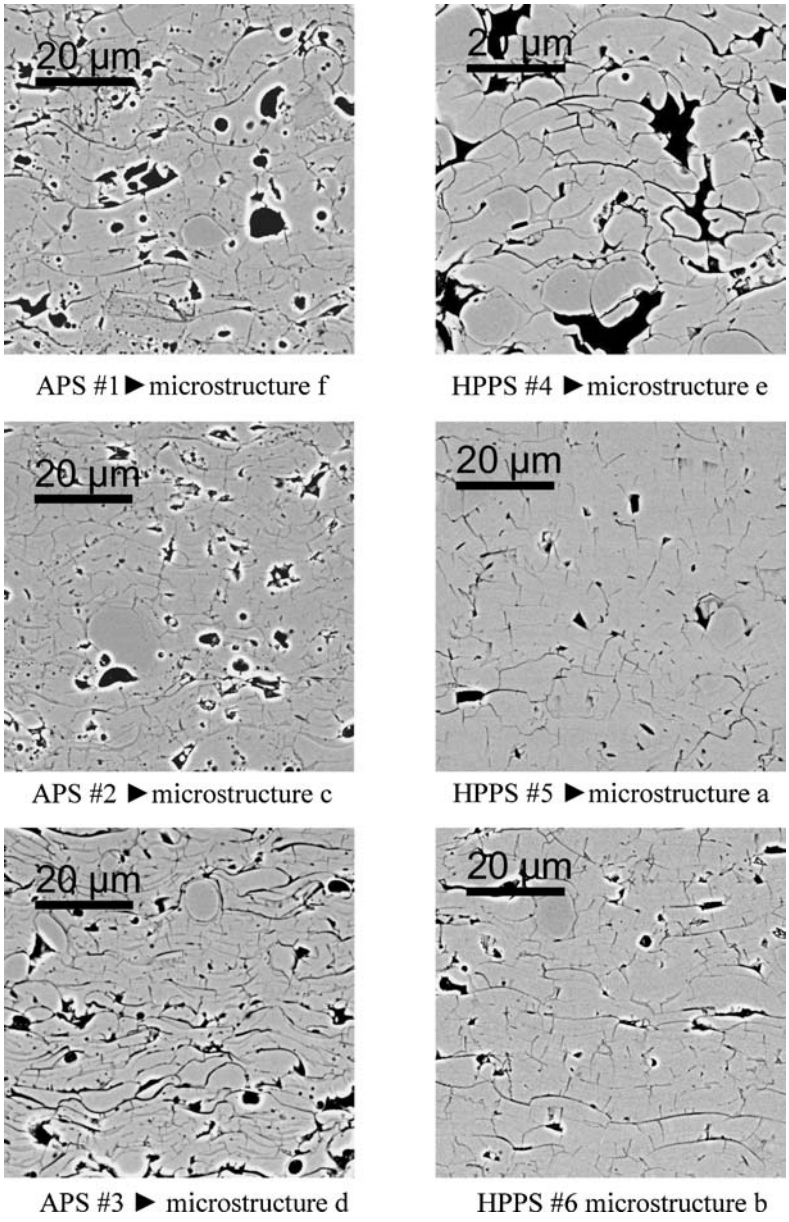

Fig. 3. Back-scattered images of selected alumina coatings; cross-sections.

powder No. 2 (microstructure c). The APS spraying of the fine powder No. 3 ($-12+2$ μm) lead to the highest amount of inter-lamellar defects. Moreover, all coatings exhibit densities of inter-lamellar defects higher than the intra-lamellar ones except for the most dense coating sprayed in the HPPS mode (HPPS #5) with powder No. 2 (microstructure a). In this case, a very good contact between lamellae was observed.

3.2. Dielectric Properties

Absorbed Current Method: Six series of ten electrons injections were made on the outer surface of as-sprayed alumina coatings. Q_{ab}, Q_r and t_r have been deduced from the $I_{ab}(t)$ experimental plots. The representative $I_{ab}(t)$ graphs obtained for each microstructure (a to f) with increasing defects content (pores and cracks) are given on Fig. 5.

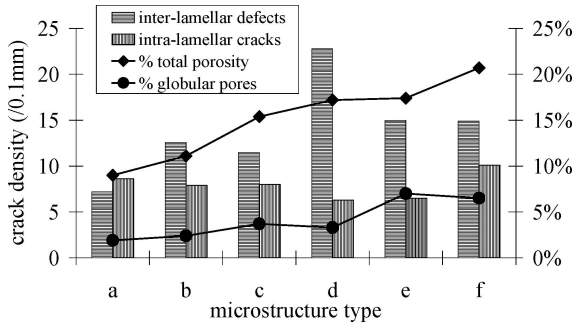

Fig. 4. Porosity contents (globular and total) and crack densities (intra- and inter-lamellar) of the six selected alumina coatings.

The most dense coating (microstructure a, Fig. 5(i)) exhibited $I_{ab}(t)$ plot with a continuous profile. It showed that such microstructure was able to store a large amount of charges. Three main trapping steps could be noticed:

- *step A*: a drastic increasing of I_{ab} was recorded that corresponded to a rapid trapping of incident electrons during the first milliseconds. As the negative charges built up in the insulator, a negative surface potential appears at the insulating surface.
- *step B*: a slow and continuous decreasing of I_{ab} was observed up to 40ms. The incident electrons were slowed down or deflected in the surrounding area of the initial irradiated zone owing to the surface potential. The secondary emission yield is increased and the quantity of stored charges decreased.
- *step C*: an asymptotic profile was observed. It corresponds to a self-regulating process between slowing of incident electrons, secondary emission (out coming electrons), diffusion and trapping of charges.

This material might be considered as a good insulator, a rather constant flow rate of electrons could be

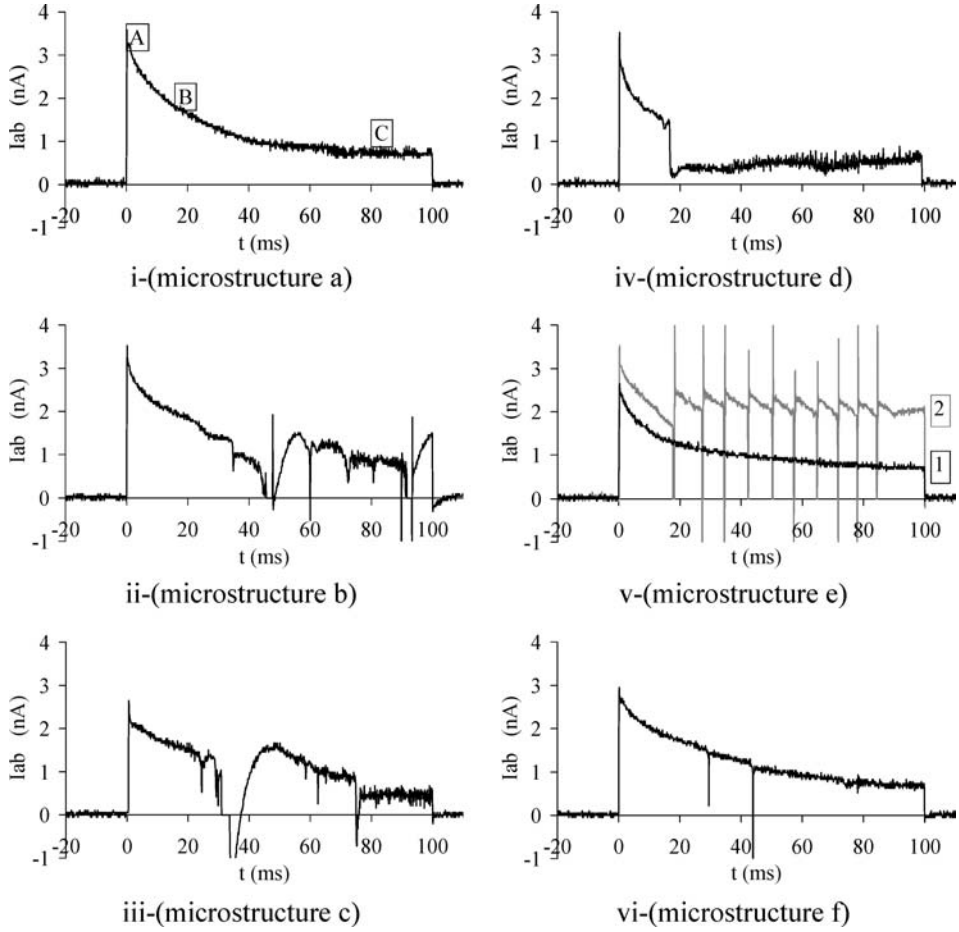

Fig. 5. Typical absorbed-current curves (i to vi) obtained during injections on the surfaces of the different microstructures (a to f).

maintained without sudden relaxation. In such a case, Q_{ab}, t_r and Q_r could be calculated with a good statistic.

The five other coatings microstructures (Fig. 5(b) to (f)) mostly exhibited relaxations during injection. As pertinent parameters t_r and Q_r were chosen in these cases. From the $I_{ab}(t)$ curves shape it follows:

– The steps A and B (rapid trapping and slow decreasing of I_{ab} up to t_r) were rather similar for all samples. It means that the main difference between the microstructures concerned the step C.
– Microstructures (b) and (c) showed numerous relaxations (for 9 times out of 10, relaxations were monitored, the rest was with a stabilized current) that evidenced a poor ability to store charges. The relaxations occur when the induced internal electric field becomes strong enough, higher than the critical detrapping energy needed to destabilize the trapped charges.
– The microstructure (d) exhibited only a single relaxation followed by a stabilized low I_{ab} value, around 500 pA (for 7 times out of 10, a single relaxation was monitored; the rest was with a stabilized current).
– In case of microstructure (e), half of the curves was with a continuous I_{ab} profile (see label 1 in Fig. 5(v)). The other profiles exhibited a particular shape with periodic relaxations (around every 10 ms) resulting in a non stabilized high I_{ab} value, around 2000 pA (see label 2 in Fig. 5(v)).
– Despite the presence of numerous defects, the most porous coating (microstructure f) showed a similar behaviour than the most dense one (only rare relaxations were detected in this case).

The results given by the absorbed current experiments performed on the surface of as-sprayed alumina coatings can be summarized regarding the influence of porosity level, cracks content and cracks orientation, Fig. 6.

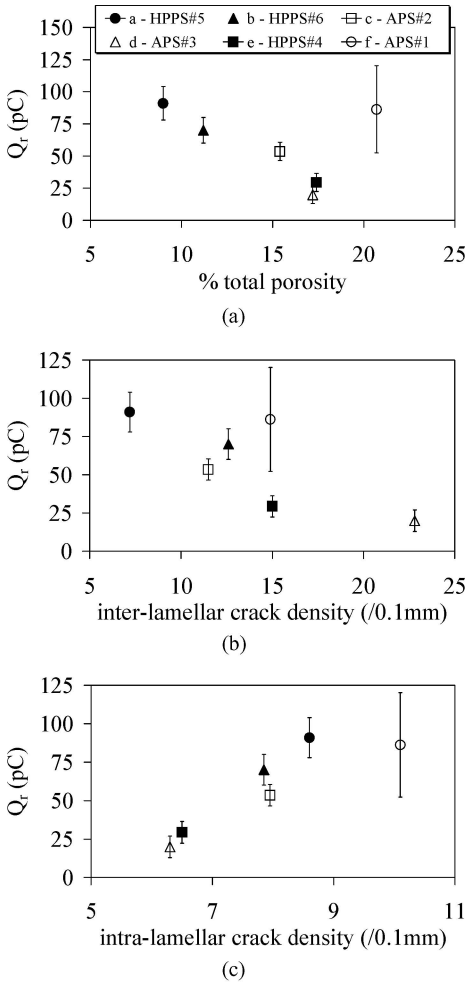

Fig. 6. Evolution of Q_r parameter measured on alumina coatings surface vs. (a) porosity content, (b) inter-lamellar cracks content, (c) intra-lamellar cracks content.

If total porosity content is considered, Q_r (and also t_r) was always low as the coating was porous except for the most porous one (microstructure f) (Fig. 6(a)). This result showed that the defects (pores and cracks) act as diffusion barriers for electrons and limit the electrons propagation within the whole coating. The lowest Q_r value for microstructure d could be explained by the presence of highly numerous inter-lamellar defects perpendicular to the direction of injection. Moreover, the high Q_r rate obtained for the microstructure f corresponds to the coating with the highest intra-lamellar cracks content (parallel to the injection direction). When Q_r was plotted according to the two crack orientations (Fig. 6(b) and (c)), it was obvious that Q_r was always low as the inter-lamellar cracks content was high and as the intra-lamellar cracks content was low. So, evidence is done that electrons move preferentially through the defects (intra-lamellar cracks) parallel to the direction of injection. The same trend was observed with t_r.

Microstructure e exhibits large pores with size of the same order of magnitude than the size of the area irradiated during SEMME experiments. In this case, the two different behaviour modes observed (Fig. 5(v)) could be explained by the location of injection either in a dense alumina area (curve 1) or

near by the large pores leading to numerous relaxations (curve 2).

To confirm the role of cracks as pathway or barrier for the diffusion of electrons, injections were made on the cross-sections of the two dense coatings having different crack orientations. In the first case the cracks are mainly inter-lamellar and parallel to the coating surface (microstructure b); in the second case the cracks are mainly intra-lamellar and perpendicular to the coating surface (microstructure a). It has been shown that the trapping characteristics (Q_{ab}, Q_r and t_r) are independent of coating as well as localization of injection (surface or cross section.). Nevertheless, when injections are made perpendicularly to the main orientation of defects, numerous relaxations occurred. For injections made in the direction of cracks no relaxation appeared. These results are in good agreement with the previous ones made on the coating surface. This non-isotropic dielectric behaviour revealed by the SEMME experiments is summarized in Fig. 7.

Mirror Method: All the coatings investigated exhibit a mirror effect indicating that local charge trapping is the preponderant mechanism by comparison with the charge diffusion mechanism. Nevertheless, if relaxations occur during injection, as previously shown, an unknown part of charges is re-emitted in the vacuum SEM chamber. Consequently, in such case, even if the mirror effect was observed, the quantity Q_t deduced from the slope of the linear part of the curve $1/d = f(V)$, cannot be an measured accurately [12].

A typical "mirror plot" is given on Fig. 8. The curved part of the plot is associated with a spreading of charges within the surface since the curve is located under the straight line [13]. When accurate measurements can be done, the values of Q_t obtained confirm the influence

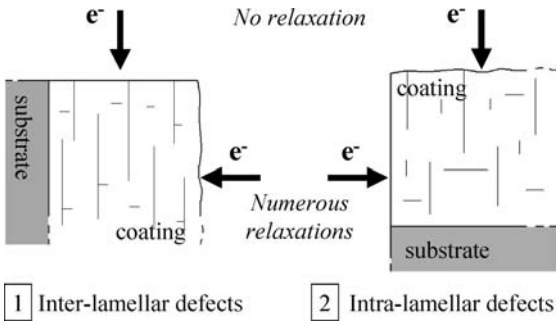

Fig. 7. Schematic representation of the influence of the defects orientation on the relaxation occurrence.

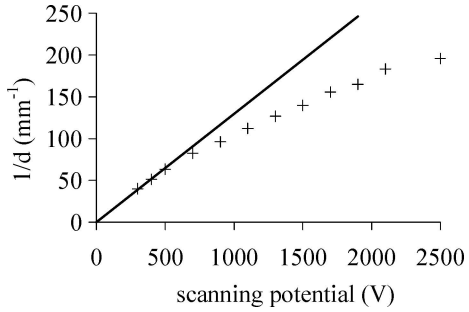

Fig. 8. Experimental mirror plot obtained after 500 pC injected electrons. Calculated trapped charge from the linear part of the plot: Q_t = 54 pC. Q_{ab} from the absorbed current measure is 138 pC.

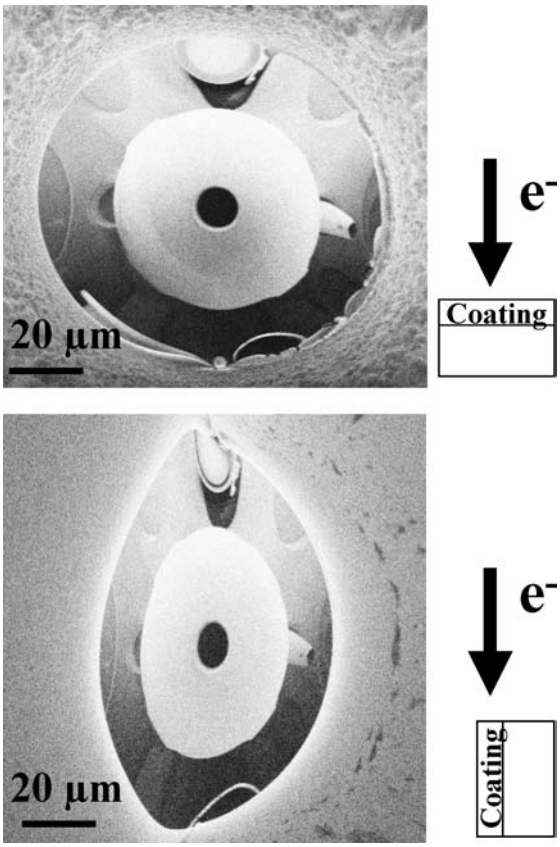

Fig. 9. Mirror images obtained at 700 V after injection (a) on the surface (b) on the cross-section.

of defects orientation on the trapping ability of coatings as previously shown with the absorbed current measurements.

An example of the mirror images obtained after injections is given on Fig. 9. Injections made on the

coating surface lead to usual circular mirror shape. On the contrary, an unusual elliptic mirror shape is observed when injection is performed on the cross-sections of the coatings. This trapping anisotropy can be related to the anisotropy of the coating. It had confirmed and illustrated that electrons were preferentially spreaded along the lamellae than across the coating and through the inter-lamellar voids.

4. Conclusion

The SEMME method (absorbed current and mirror measurements) has been successfully applied to the characterisation of the behaviour of charges in plasma-sprayed alumina coatings.

It has been shown that the structure of the thermally-sprayed coatings (lamellar and oriented) is responsible for an anisotropy of the trapping, diffusion and spreading of charges. Whatever the microstructure the mechanism involved for the trapping saturation (Step C in Fig. 5) seems to be always the same. On the contrary, according to the microstructure, different detrapping processes occur (Step B): the soft detrapping, associated with a self regulating mechanism (diffusion, secondary emission, trapping. . .) and a sudden detrapping characterised either by strong random relaxations or by strong periodic relaxations.

One of the most important results to be underlined is the influence of the defects, namely pores and cracks. Defects act as pathway for the charges diffusion when the direction of injection is parallel to the main cracks orientation, but as barrier when the direction of injection is perpendicular to the crack orientation.

SEMME method is a powerful tool to investigate the ability of trapping – detrapping of charges in ceramic coatings. It can help towards spraying ceramic coatings with good insulating properties, that is coatings able to regulate the amount of trapped charges without any damage. Both alumina powders and plasma parameters can be chosen to obtain microstructures leading to either a soft or a periodic sudden detrapping of charges.

As a lot of properties of insulating materials are linked to the stored charges, further investigations are needed to determine the performance of such ceramic coatings against breakdown, ageing or under mechanical (for example) exposure.

Acknowledgments

Mrs De Dave-Fabregue and Mr Borit from the 'Ecole des Mines de Paris' are gratefully acknowledged for their work (microstructural analyses and CAPS spraying). Researchers of the 'Ecole Centrale de Lyon' are gratefully acknowledged for their help for the SEMME experiments.

References

1. R. Gadow, A. Killinger, and V.C. Friedrich, in *Meeting the Challenges of the 21th Century*, edited by C. Coddet (Pub ASM Int., Materials Park, OH, 1998), p. 1083.
2. T. Paul, R. Hartmann, J. Heberlein, K.H. Schoenbach, W. Shi, and R. Stark, in *Proceedings of the ITSC2002*, edited by E. Lugscheider (Pub. DVS-German Welding Society, Düsseldorf, 2002), p. 793.
3. L. Golonka, and L. Pawlowski, *Electrocomp. Sc. Technol*., **10**, 143 (1983).
4. M. Fasching, F.B. Prinz, and L.E. Weiss, *J. Therm. Spray Technol*., **4** (2), 133 (1995).
5. L. Pawlowski, *Surf. Coat. Technol*., **35**, 285 (1988).
6. C.J. Swindeman, R.D. Seals, W.P. Murray, M.H. Cooper, and R.L. White, R. L, Practical Solutions for Engineering Problems, edited. C.C. Berndt (Pub ASM Int., Materials Park, OH, 1996), p. 793.
7. C. Friedrich, R. Gadow, and A. Killinger, in *Proceedings of the UTSC99*, edited by E. Lugscheider and P. A. Kammer (Pub DVS-German Welding Society, Düsseldorf, 1999), p. 676.
8. E. Rajamäki, T. Varis, A. Kulkarni, J. Gutleber, A. Vaidya, M. Karadge, S. Sampath, and H. Herman, in *Proceedings of ITSC2002*, edited by E. Lugscheider (Pub DVS-German Welding Society, Düsseldorf, 2002), p. 622.
9. A. Kulkarni, S. Sampath, A. Goland, H. Herman, and D. Dowd, *Script. Mat.*, **43**, 471 (2000).
10. S. Beauvais, V. Guipont, F. Borit, M.. Jeandin, M. Español, K. Khor, A. Robisson, and R. Saenger, *Surf. Coat. Technol*., **183**, 204 (2004).
11. S. Beauvais, PhD thesis, Ecole des Mines de Paris, (2003) (in French).
12. B. Vallayer, G. Blaise, C. Le Gressus, and D. Tréheux., *Rev. Scient. Instr*., **70**(7), 3102 (1999).
13. J. Bigarré, C. Attard, P. Hourquebie, and J. Matallana, *IEEE, Trans. Dielec. Insul.*, **8**(6), 942 (2001).
14. J. Liebault, J. Vallayer, D. Goeuriot, D. Treheux, and F. Thevenot, *J. Eur. Ceram. Soc*., **21**, 389 (2001).
15. O. Morey, P. Goeuriot, D. Juve, and D. Treheux, *J. Eur. Ceram. Soc*., **23**, 345 (2003).
16. G. Blaise, in *Proceedings of CEIDP '93, Annual report*, edited by IEEE (1993) p. 98.